Research Article

Xinli Zhao, Zhengming Yang, Xuewei Liu*, Zhiyuan Wang, and Yutian Luo

Analysis of pore throat characteristics of tight sandstone reservoirs

https://doi.org/10.1515/geo-2020-0121
received April 10, 2020; accepted July 13, 2020

Abstract: The characterization of pore throat structure in tight reservoirs is the basis for the effective development of tight oil. In order to effectively characterize the pore -throat structure of tight sandstone in E Basin, China, this study used high-pressure mercury intrusion (HPMI) testing technology and thin section (TS) technology to jointly explore the characteristics of tight oil pore throat structure. The results of the TS test show that there are many types of pores in the tight sandstone, mainly the primary intergranular pores, dissolved pores, and microfractures. Based on the pore throat parameters obtained by HPMI experiments, the pore throat radius of tight sandstone is between 0.0035 and 2.6158 μm. There are two peaks in the pore throat distribution curve, indicating that the tight sandstone contains at least two types of pores. This is consistent with the results of the TS experiments. In addition, based on the fractal theory and obtained capillary pressure curve by HPMI experiments, the fractal characteristics of tight sandstone pore throat are quantitatively characterized. The results show that the tight sandstones in E Basin have piecewise fractal (multifractal) features. The segmentation fractal feature occurs at a pore throat radius of approximately 0.06 μm. Therefore, according to the fractal characteristics, the tight sandstone pore throat of the study block is divided into macropores (pore throat radius > 0.06 μm) and micropores (pore throat radius < 0.06 μm). The fractal dimension D_L of the macropores is larger than the fractal dimension D_S of the micropores, indicating that the surface of the macropores is rough and the pores are irregular. This study cannot only provide certain support for characterizing the size of tight oil pore throat, but also plays an inspiring role in understanding the tight pore structure of tight sandstone.

Keywords: tight sandstone, high-pressure mercury intrusion, thin section, pore throat structure, fractal dimension, E Basin

*** Corresponding author: Xuewei Liu,** Institute of Porous Flow and Fluid Mechanics, University of Chinese Academy of Sciences, Langfang, 065007, People's Republic of China; Research Institute of Petroleum Exploration & Development, PetroChina Company Limited, Beijing, 100083, People's Republic of China, e-mail: lxw69@petrochina.com.cn
Xinli Zhao: College of Engineering Science, University of Chinese Academy of Sciences, Beijing, 100049, People's Republic of China; Institute of Porous Flow and Fluid Mechanics, University of Chinese Academy of Sciences, Langfang, 065007, People's Republic of China; Department of Porous Flow & Fluid Mechanics, Research Institute of Petroleum Exploration & Development, PetroChina Company Limited, Langfang, 065007, People's Republic of China, e-mail: zhaoxinli17@mails.ucas.edu.cn
Zhengming Yang, Yutian Luo: University of Chinese Academy of Sciences, Beijing, 100049, People's Republic of China; Institute of Porous Flow and Fluid Mechanics, University of Chinese Academy of Sciences, Langfang, 065007, People's Republic of China; Department of Porous Flow & Fluid Mechanics, Research Institute of Petroleum Exploration & Development, PetroChina Company Limited, Langfang, 065007, People's Republic of China
Zhiyuan Wang: Institute of Oceanography, Minjiang University, Fuzhou, 350108, People's Republic of China
ORCID: Xinli Zhao 0000-0002-0367-5092

1 Introduction

As an unconventional oil and gas resource, tight oil and gas has received more and more interest in researchers [1,2]. In China, tight sandstones are defined as reservoirs with the porosity of <10%, and gas permeability $<1 \times 10^{-3}$ μm^2 [3,4]. The tight reservoir has extremely low porosity and permeability, so it has no natural capacity. Generally, the development of tight oil requires volumetric fracturing to obtain an industrial oil stream [5]. In addition, the pore throat structure is a significant parameter affecting the seepage of tight oil during the development [6–9]. However, characterizing the multiscale (nano-millimeter) pore throat structure distribution system of tight sandstones is a difficult research point.

For now, the techniques for the characterization of tight oil pore throat structure mainly include rate-controlled mercury intrusion (RCMI), high-pressure mercury intrusion (HPMI), low-temperature nitrogen adsorption (LTNA),

scanning electron microscope (SEM), thin section (TS), X-ray computer tomography (CT), and nuclear magnetic resonance (NMR) techniques [10–20]. However, various technologies just mentioned have their respective advantages and disadvantages in practical applications [21]. For example, RCMI technology can obtain pores and throats in tight sandstones according to its testing principles, but it can only test pore throats larger than 0.1 μm [22]. The LTNA technology can only test the pores of less than 100 nm in tight sandstone and its accuracy in calculating the pore radius depends on the choice of the calculation model [23–25]. In addition, NMR technology can perform nondestructive testing of the pore throat radius distribution characteristics of the porous media, but the conversion of the T2 spectrum (transverse relaxation time) into the pore throat radius distribution requires a combination of other testing techniques (such as RCMI) [26]. SEM, TS, and CT techniques can qualitatively and intuitively observe information such as pore throat size, connectivity, and pore throat type in rocks [27–29]. In addition, SEM technology can also obtain information on the composition of minerals in rocks, which is widely used to analyze the petrological characteristics of tight sandstones. Therefore, in order to accurately characterize the distribution characteristics of multiscale pore throat structures in tight sandstones, a technique capable of testing the full range should be proposed. The HPMI is carried out by injecting a nonwetting phase (mercury) into a tight sandstone core by high pressure to obtain a distribution of pore throat radius in the core. The test range is from nanometer to micrometer, which can describe the distribution characteristics of tight sandstone pore throat radius. Additionally, this technology has been widely used in the study of rock pore throat structures and numerous successful applications of HPMI technology have already shown its efficiency for pore throat characterization [30–32].

Fractal geometry is an effective means of describing irregular objects in nature [33]. Since its development and promotion by Mandelbrot and Wheeler in 1983, many scholars have successfully applied it to the petroleum industry to study the fractal features of complex and irregular pore throat structures in porous media [34–36]. In addition, with the exploration and development of tight oil, many scholars use fractal theory to quantitatively characterize the tight sandstone nanoscale pore throat network system [37,38]. It is found that the complex pore throat structure of tight sandstone has fractal characteristics, and its fractal dimension is large, which has the characteristics of segmentation and fractal [39,40]. It indicates that the tight sandstone pore throat surface is irregular, rough, and heterogeneous. Moreover, the classification of pore throat size for tight sandstones is also a part of the exploration phase. Although some scholars and institutions have proposed some classification methods for pore throat size, the tight sandstones for specific blocks need to be classified according to their own characteristics. For example, in the pore throat size classification method proposed by the International Union of Pure and Applied Chemistry, micropores are less than 2 nm in width, mesopores in the range of 2 to 50 nm in width, and width of the macropores is greater than 50 nm [41]. This classification method is widely used in the pore throat radius distribution of shale. Nevertheless, in the study of tight oil, this classification method almost divides all pores into large pores. This is definitely not accurate enough in the petroleum industry [42]. Additionally, in terms of rock pore size classification, Pittman proposed an empirical formula for predicting the pore distribution curve based on the experimental data of 202 core samples [43]. Loucks et al. extended Choquette and Pray's pore size classification for carbonates and proposed a new pore size classification scheme. In this scheme, nanopores range from 1 nm to 1 μm, micropores range from 1 to 62.5 μm, and mesopores from 62.5 μm to 4 mm [44]. However, for tight oil pore throat radius is generally less than 1 μm, this method has certain limitations in the classification of pore throats of tight sandstone. As the tight sandstone has the characteristics of segmentation and fractal, according to the critical point of the segment the pore throat size can be classified.

In this study, HPMI and TS experiments were carried out using the tight oil cores of the drilled E Basin. The TS can visually observe the pore throat type in the core and characterize the core pore throat structure qualitatively. In addition, based on the HPMI experiment, this paper used the fractal theory to quantitatively characterize the pore throat structure of tight sandstone.

2 Samples

The core samples of tight sandstone selected in this study are taken from Honghe Oilfield and Weibei Oilfield in E Basin, China. The tight sandstones in the E Basin mainly include lithic arkose sandstones and feldspathic litharenite sandstones, according to Folks classification (see Figure 1). And, their relative content accounts for about 50%. Detailed information of 12 core samples is shown in Table 1. The permeability of the core sample is between 0.202×10^{-3} μm^2 and 1.785×10^{-3} μm^2 with an average of 0.558×10^{-3} μm^2. And, the core samples have a porosity between 7.6% and 12.9% with an average of

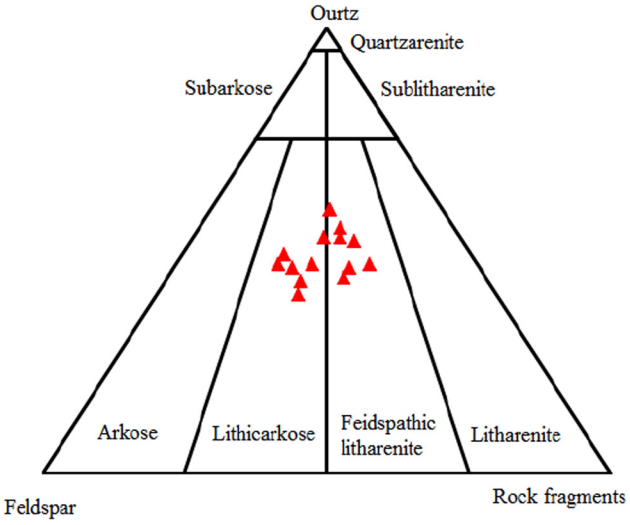

Figure 1: Triangular diagram of rock composition of tight sandstone reservoir in E Basin.

10.2%. Therefore, according to Chinese petroleum industry standards, these cores are typical tight sandstones.

3 Test and calculation method

3.1 HPMI and TS

The HPMI is based on a capillary beam model and assumes that the porous medium consists of capillary bundles of different diameters. The main measured value of the HPMI test is the mercury inlet pressure (corresponding to the throat radius) and mercury saturation (corresponding to pore throat volume). The HPMI equipment, named AutoPore IV 9520, was used to measure pore throat size and the maximum mercury pressure can reach about 206 MPa, corresponding to a pore throat radius of 3.5 nm. After the experiment reached the highest mercury inlet pressure, the pressure gradually decreased and mercury withdrew the core sample. In the HPMI experiment, the mercury injection and withdrawal capillary pressure curves were obtained and the pore throat characteristics of the tight sandstone were analyzed based on this. In addition, in this experiment, the temperature in the laboratory was 21°C and the humidity was 60%. At the same time, the capillary pressure curve can characterize the pore throat structure feature, because the capillary pressure is mainly controlled by pore throat network sorting and pore throat size. Through the relationship between capillary pressure (P_c) and pore throat radius (r), the curve of pore throat radius was obtained to assess the pore throat structure of the tight sandstone. Its calculation formula is as follows [45]:

$$P_c = \frac{2\sigma \cos\theta}{r} \quad (1)$$

where P_c is the capillary pressure in MPa, σ is the surface tension of air/mercury in N/m, θ is the contact angle in °, and r is the pore throat radius in μm. In addition, the surface tension of air/mercury is 485 mN/m and the contact angle is 140°.

In the TS method, the colored (red or blue) liquid glue is injected into the pores of rock under vacuum or pressure and ground it into thin slices after solidification by liquid gel. It is easy to identify under the microscope when the pores in the rock are filled with nonferrous glue. The information of pore distribution, type, development degree, and geometric shape can be observed

Table 1: Information of experimental core samples

Sample	Well	Depth (m)	Subsection	Porosity (%)	Perm (10^{-3} μm^2)
WB49-66	WB49	569.81	Weibei	11.2	0.216
WB49-80	WB49	569.99	Weibei	12.0	0.393
WB14-59	WB14	570.16	Weibei	11.2	0.497
WB14-13	WB14	570.38	Weibei	12.1	0.399
WB49-53	WB49	570.84	Weibei	10.5	1.785
WB49-72	WB49	571.02	Weibei	9.1	0.202
HH153-10	HH153	2097.48	Honghe	8.3	0.223
HH153-61	HH153	2097.90	Honghe	10.6	1.04
HH153-66	HH153	2098.26	Honghe	9.8	0.769
HH153-80	HH153	2098.76	Honghe	7.6	0.341
HH153-91	HH153	2099.40	Honghe	9.5	0.530
HH153-100	HH153	2100.04	Honghe	8.9	0.295

directly in the core slice. In this study, the LEICA DMRXHC multifunctional polarizing microscope was used in the experiment of TS, and the information of pore type was observed.

3.2 Fractal dimension calculation

Fractal theory has been widely used in petroleum engineering since its establishment in the mid-1970s. It is studied in a disorderly and self-similar system that is widespread in nature. As a porous medium, rock's pore throat system has self-similar properties. Li derived the calculation formula of fractal dimension based on the capillary model and studied the rock heterogeneity [46]. Wang et al. believe that different pore distribution characteristics of tight sandstones have different calculation methods of fractal dimension [47]. The previous studies have found that there is a relationship between pore volume, pore radius, and fractal dimension as described as follows:

$$V \propto r^{3-D} \tag{2}$$

where V is the rock pore volume, m^3; r is the pore radius, m; and D is the fractal dimension.

Deriving the derivative of equation (2), the following is obtained:

$$\frac{dV}{dr} \propto r^{2-D} \tag{3}$$

By integrating equation (3), an expression for the cumulative pore volume ($V(>r)$) with a pore radius greater than r is obtained:

$$V(>r) = \int_{r}^{r_{max}} \alpha r^{2-D} dr = \beta(r_{max}^{3-D} - r^{3-D}) \tag{4}$$

where r_{max} is the maximum pore radius, m; α and β are the proportional constants, $\beta = \alpha/(3 - D)$.

If the maximum pore radius and the minimum pore radius in the pore are known, the pore volume is calculated as follows:

$$V = \beta(r_{max}^{3-D} - r_{min}^{3-D}) \tag{5}$$

where r_{min} is the minimum pore radius, m.

The cumulative volume fraction (S) can be expressed as follows:

$$S = \frac{V(>r)}{V} = \frac{r_{max}^{3-D} - r^{3-D}}{r_{max}^{3-D} - r_{min}^{3-D}} \tag{6}$$

The minimum pore radius in tight sandstone is much smaller than the maximum pore radius, i.e., $r_{min} \ll r_{max}$. Therefore, S can be reduced to the following formula:

$$S = 1\left(\frac{r}{r_{max}}\right)^{3-D} \tag{7}$$

Assuming that the contact angle is not affected by the pore throat size, then the fractal formula of pore throat radius distribution can be obtained.

$$S = 1 - \left(\frac{P_c}{P_{min}}\right)^{3-D} \tag{8}$$

where s is the volume of mercury entering the pores in the HPMI experiment, %; P_c is the capillary pressure, MPa; and P_{min} is the capillary pressure corresponding to the maximum pore throat radius r_{max} (*i.e.*, capillary pressure of entrance).

Taking the logarithm of the two sides of equation (8) can get the following formula:

$$\log(1 - s) = (D - 3)\log P_c - (D - 3)\log P_{min} \tag{9}$$

In the HPMI test, 1-s represents the saturation of the wetted phase, which can be expressed in S_w. Therefore, equation (9) can be expressed as follows:

$$\log S_w = (D - 3)\log P_c - (D - 3)\log P_{min} \tag{10}$$

Based on the HPMI experiment, the fractal dimension of the rock pore throat network system can be calculated according to equations (9) and (10) and the microstructure characteristics of the porous medium also can be described.

4 Results

4.1 Petrological characteristics and pore throat types

There are various types of cuttings, mainly metamorphic rocks and sedimentary rocks, including igneous rocks and mica, and the soft rock cuttings are pseudo-matrix. Interstitials include heterobases and types of cement with a low volume fraction, generally less than 10%, with an average of 8.6%. The heterogeneous base is mainly muddy (Figure 2b and d). Some of the muddy rock fragments are rich in organic matter and the compacted deformation is pseudo-matrix. The cement is made of mainly calcite and dolomite and contains a small amount of quartz, feldspar, pyrite, and kaolinite.

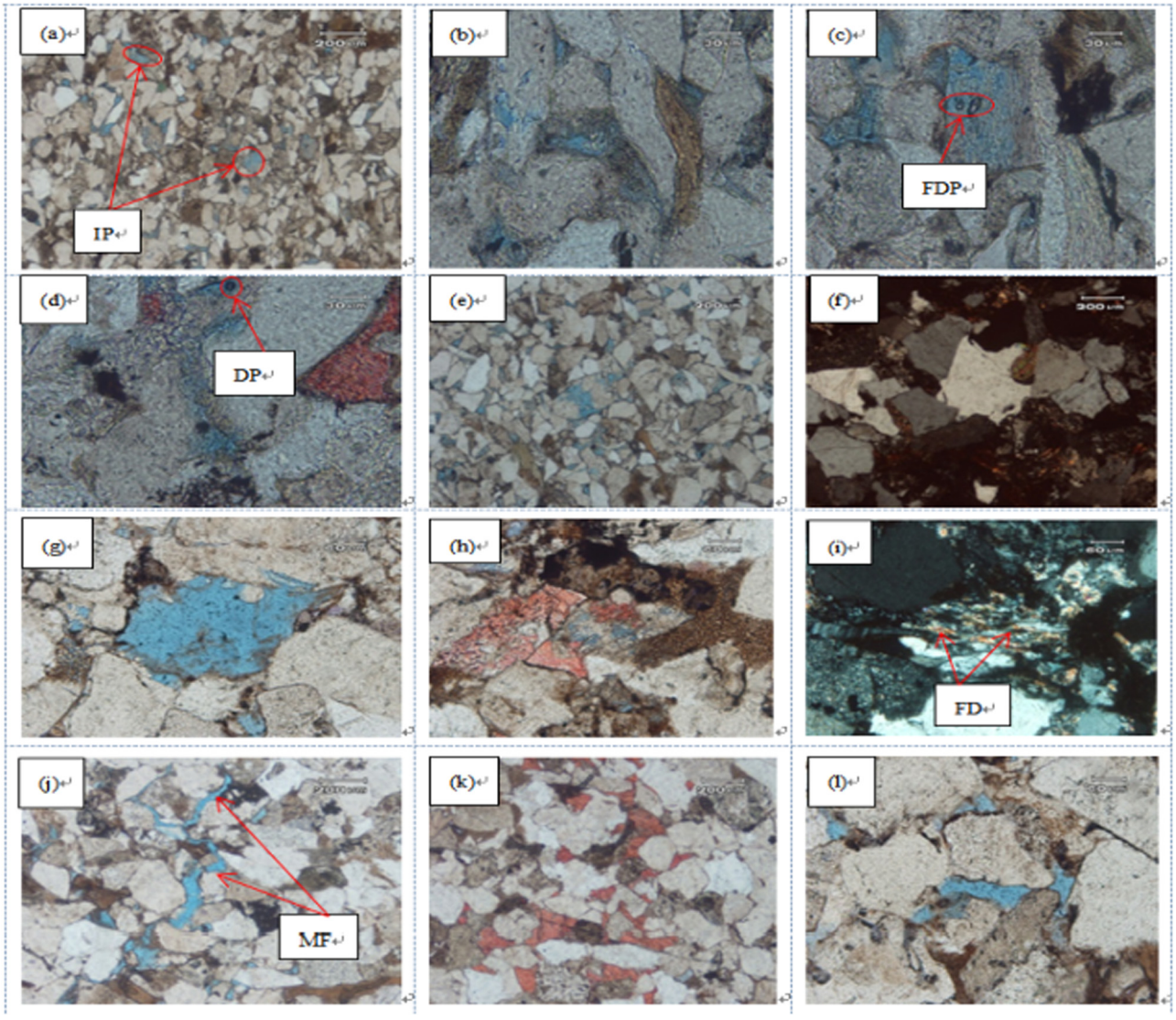

Figure 2: Tight sandstone TS analysis of the type of pore throat. (a) Intergranular pore, moldic pore (WB49-66, 569.81 m); (b) dissolved pore of mudstone (WB49-66, 569.81 m); (c) feldspar dissolved pore (WB49-66, 569.81 m); (d) kaolinite dissolved pore, calcite, heterogroup (WB49-80, 569.99 m); (e) feldspar dissolved pore, intergranular pore (WB14-59, 570.16 m); (f) quartz overgrowth (HH153-100, 2100.04 m); (g) moldic pore (HH153-100, 2100.04 m); (h) cementation metasomatism of calcite, intragranular dissolved pore (HH153-100, 2100.04 m); (i) flake debris (HH153-100, 2100.04 m); (j) solution microfracture (HH153-100, 2100.04 m); (k) calcite (HH153-100, 2100.04 m); (l) intergranular pore (HH153-100, 2100.04 m). IP, intergranular pore; FDP, feldspar dissolved pore; DP, dissolved pore; FD, flake debris; MF, microfracture.

Quartz is mainly single-crystal quartz, and most of them are subribbed. The types of pores include primary pores, secondary pores, heterobasic pores, and microfractures. The pores are mainly triangular and multilateral intergranular pores, and some intergranular pores are enlarged by dissolution. Among them, the intergranular filling is mixed with chlorite, calcite, dolomite, and a small amount of heavy oil (Figure 2c). At the same time, it was found that there were under-developed pores and uneven distribution, which were isolated fine intergranular pores. Its pore size is 0.05–0.20 mm and the maximum is 0.38 mm (Figure 2l). Followed by feldspar and mudstone debris (Figure 2h), there are mold pores also (Figure 2g), the general diameter of 0.05–0.12 mm and the maximum of 0.18 mm. The characteristics of the pore throat are mainly point-shaped pore throat, a small number of thin tubular and flaky. The other type is feldspar formed by dissolution, dissolved pores in rock fragments and a small number of miscellaneous pores. The pore coordination number is 0–2. There is a point-like pore

throat in the sandstone of the study block, and the local dissolution crack is 0.025–0.75 mm (Figure 2j). Although the development of fractures has little effect on increasing reservoir space, it can significantly improve reservoir seepage capacity [48,49]. In addition, the particle size is mainly in fine sand–fine sand (Figure 2a–e) and medium sand–fine sand grade (Figure 2f–l). In this study, the rock sorting performance of the tight reservoir in the block is moderate–good. The rounding is usually shown as an angular–secondary angular shape, and the particles are mainly dominated by line contact. The types of cementation are film – pore and film – embedded crystal type.

4.2 Distribution characteristics of pore throat

The distribution curve of the pore throat radius was obtained by HPMI experiment (Figure 3). The pore throat radius distribution curve shows multiple peaks. It suggests that there are multiple kinds of pore types in the tight sandstone, which is consistent with the results obtained by the TS experiment (Figure 2). In addition, the existence of multiple peaks in the pore throat distribution curve suggests that the tight sandstone in the target reservoir is highly heterogeneous. In Figure 3a, the first peak is between 0.0035 and 0.01 μm and the second peak is between 0.01 and 2.615 μm. However, in Figure 3b, the first peak is between 0.0035 and 0.0408 μm and the second peak is between 0.0408 and 2.615 μm. Besides, with the increase of permeability, the pore throat distribution curve shows a trend of gradually moving to the right. The pore throat radius of the tight sandstone in the study block is between 0.0035 and 2.6158 μm, and the pore throat is well developed below 1 μm. From Figure 4, the contribution of permeability in tight sandstone that is mainly pore throat with a radius between 0.1 and 1 μm can be acquired. And with the increase of permeability, the larger pore throat radius has a greater impact on the permeability contribution. The characteristics of the tight sandstone capillary pressure curve are shown in Figure 5. The capillary pressure curve of the sample in the study area is slightly skewed, which shows that the pore throat is very small. Table 2 shows the relevant parameters of tight sandstone obtained by HPMI experiment. It is noteworthy that the threshold pressure (P_t) of the tight sandstone in the study block is mainly distributed between 0.45 and 1.47 MPa, with an average of 0.78 MPa. It has a certain negative correlation with the permeability, that is, the larger the permeability, the smaller the threshold pressure (Figure 6a). At the same

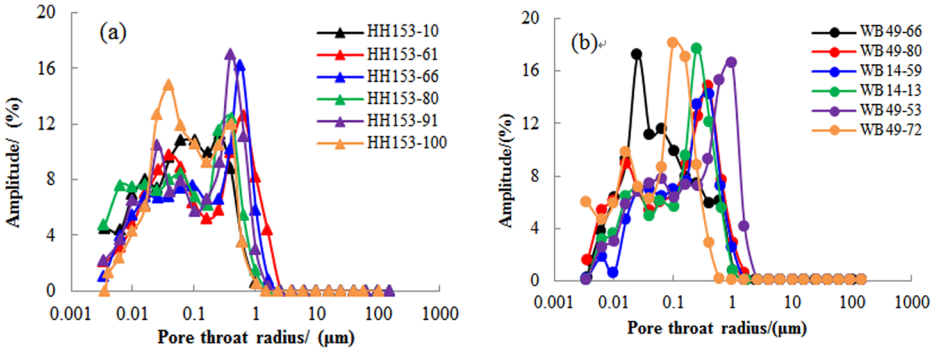

Figure 3: Pore throat radius distribution curve. (a) Honghe Oilfield; (b) Weibei Oilfield.

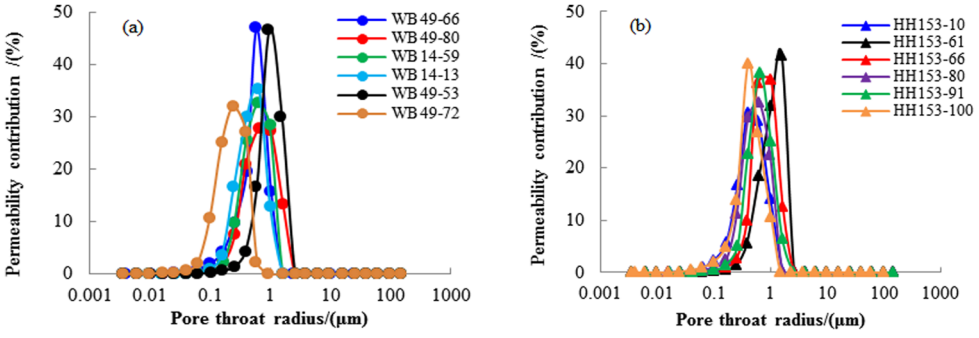

Figure 4: Permeability contribution distribution curve. (a) Weibei Oilfield; (b) Honghe Oilfield.

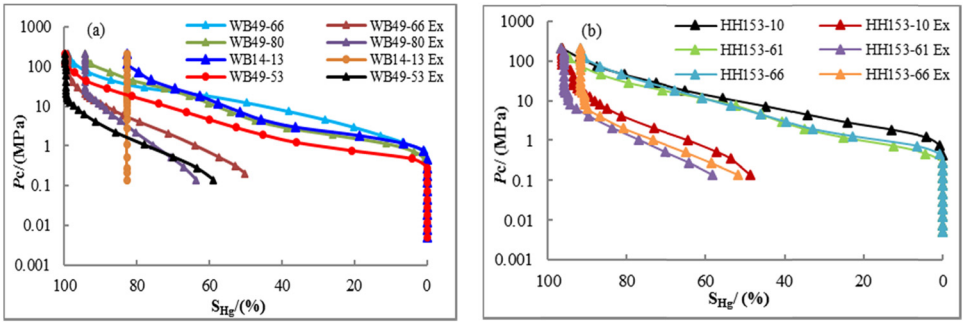

Figure 5: Mercury intrusion/extrusion curves of target reservoir in the E Basin. (a) Weibei Oilfield; (b) Honghe Oilfield.

Table 2: HPMI test results

Sample	φ	K	XP	SK	CC	CS	S_{max}	P_t	r_a	S_w
WB49-66	11.2	0.216	12.94	0.03	0.15	1.88	98.98	1.47	0.06	49.27
WB49-80	12.0	0.393	11.69	1.18	0.19	2.28	94.24	0.45	0.14	32.52
WB14-59	11.2	0.497	9.49	1.66	0.28	2.70	79.74	0.75	0.11	35.96
WB14-13	12.1	0.399	10.09	1.72	0.26	2.60	82.65	0.73	0.11	36.56
WB49-53	10.5	1.785	11.45	0.49	0.19	2.22	99.68	0.47	0.30	40.89
WB49-72	9.1	0.202	12.65	1.36	0.15	1.92	95.35	1.21	0.08	31.37
HH153-10	8.3	0.223	12.50	0.91	0.17	2.06	96.40	0.74	0.08	49.48
HH153-61	10.6	1.04	11.71	0.65	0.20	2.38	96.64	0.47	0.12	39.43
HH153-66	9.8	0.769	11.16	1.38	0.21	2.37	91.82	0.45	0.12	43.65
HH153-80	7.6	0.341	12.34	0.91	0.19	2.31	95.25	0.75	0.07	47.11
HH153-91	9.5	0.530	11.95	0.81	0.19	2.24	96.80	0.46	0.13	40.19
HH153-100	8.9	0.295	12.67	0.20	0.14	1.79	99.51	1.46	0.12	43.54

φ, porosity, %; K, permeability, 10^{-3} μm^2; XP, mean value coefficient; SK, skewness coefficient; CS, sorting coefficient; CC, variable coefficient; S_{max}, maximum mercury saturation, %; P_t, threshold pressure, MPa; r_a, median radius, μm; S_w, mercury withdrawal efficiency, %

time, there is a good positive correlation between the median radius (r_a) and the permeability (Figure 6b). This shows that the median radius has a certain degree of influence on the permeability. In addition, the tight sandstone samples in the study block have a relatively high maximum mercury saturation, which is mainly distributed between 79% and 99%. However, the mercury withdraw efficiency (S_w) is relatively low, mainly distributed in 30% to 50%, and a large amount of residual mercury saturation remains in the pores. The previous studies have suggested that this is due to the complex pore structure of the low-permeability sandstone

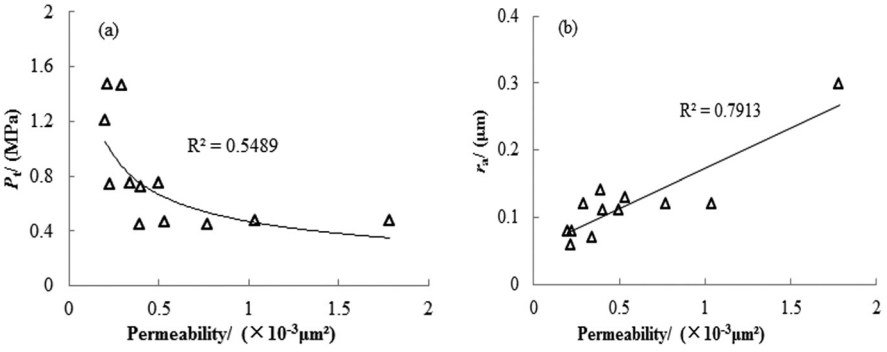

Figure 6: Relationship between permeability and threshold pressure and median radius. (a) the relationship curve between permeability and p_t; (b) the relationship curve between permeability and r_a.

reservoir, and the difference in pore and throat distribution. The retained mercury in a large number of pores is caused by the shielding effect of small pores [50].

5 Discussions

5.1 Fractal characteristics

The fractal theory is used to study the irregular elements with complex structures. Generally, fractal dimensions are used in this method to characterize object complexity. Based on the fractal dimension calculated by equations (8) and (9), the D is closer to 2, the simpler the pore throat structure, the more regular the pore throat shape. In addition, when D is closer to 3, it suggests that the more complicated the pore throat structure, the more irregular the shape. At the same time, according to the fractal theory, the fractal of pore throat structure can be divided into integral fractal (single fractal) and piecewise fractal (multifractal). The tight sandstone of this study block is characterized by multifractal, which means that there are differences in the structure of the

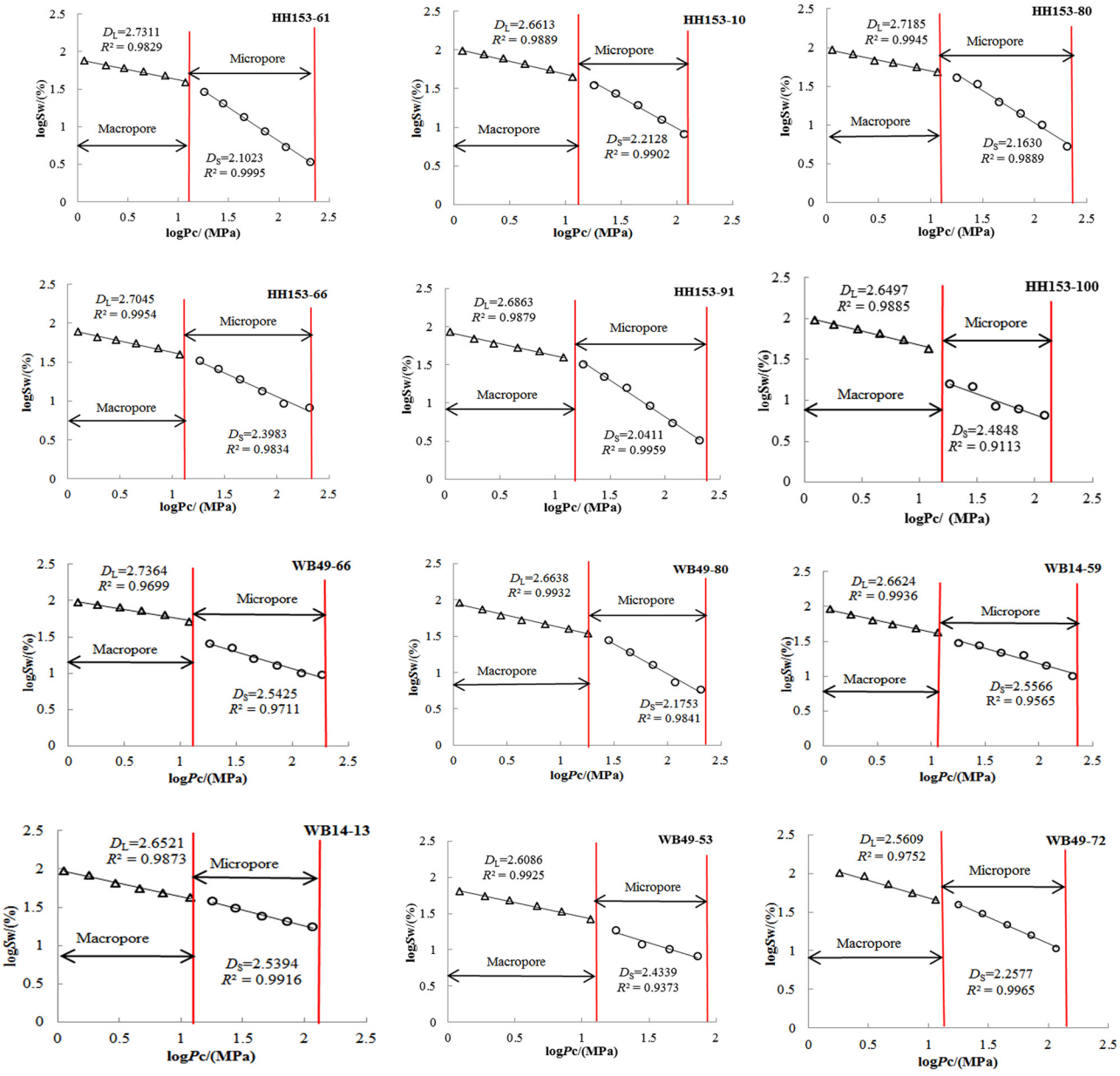

Figure 7: Fractal features of pore throat structure for tight sandstone samples.

large and small pore throats, and the fractal dimension is quite different. The tight sandstone pore throat of the E Basin has a good feature and the characteristics of segmentation fractals appear ($R^2 > 0.9$, Figure 7). Combined with the double-logarithmic curve of capillary pressure and mercury saturation obtained from the HPMI test of these sandstone cores, the curve shows a turning point at the pore throat radius of about 0.0602 μm, which is divided into two regions, indicating that the pore throat has two different scales. According to the distribution characteristics of the tight pores of the study block, the pores of these two scales can be divided into macropores (pore throat radius > 0.0602 μm) and micropores (pore throat radius < 0.0602 μm). The fractal dimension of the macropores (D_L)

Table 3: Calculation results of fractal dimension with different intervals

Sample	$K/\times 10^{-3}$ μm^2	φ/%	D_i	R^2	F_i/μm	T_r/%	D_C
WB49-66	0.216	11.2	2.7364	0.9699	0.0615–1.0375	50.12	2.6397
			2.5425	0.9711	0.0036–0.0615	49.88	
WB49-80	0.393	12.0	2.6638	0.9932	0.0613–1.6252	63.83	2.5149
			2.1753	0.9841	0.0036–0.0613	36.17	
WB14-59	0.497	11.2	2.6624	0.9958	0.0633–1.6240	82.10	2.7034
			2.5566	0.9167	0.0035–0.0633	17.90	
WB14-13	0.399	12.1	2.6521	0.9873	0.0613–1.0021	69.82	2.6332
			2.5394	0.9916	0.0035–0.0613	30.18	
WB49-53	1.785	10.5	2.6086	0.9925	0.0632–1.5735	74.26	2.5636
			2.4339	0.9373	0.0035–0.0632	25.74	
WB49-72	0.202	9.1	2.5609	0.9843	0.0621–0.9651	58.31	2.4542
			2.2577	0.9989	0.0035–0.0621	41.69	
HH153-10	0.223	8.3	2.6613	0.9826	0.0632–0.9906	67.67	2.4719
			2.2128	0.9980	0.0036–0.0632	32.33	
HH153-61	1.04	10.6	2.7311	0.9829	0.0623–1.5761	63.35	2.5006
			2.1023	0.9995	0.0035–0.0623	36.65	
HH153-66	0.769	9.8	2.7045	0.9691	0.0623–1.6506	66.41	2.6016
			2.3983	0.9834	0.0035–0.0623	33.59	
HH153-80	0.341	7.6	2.7185	0.9879	0.0633–0.9837	55.13	2.4692
			2.1630	0.9959	0.0035–0.0633	44.87	
HH153-91	0.530	9.5	2.6863	0.9879	0.0615–1.6087	62.71	2.4457
			2.0411	0.9599	0.0035–0.0615	37.29	
HH153-100	0.295	8.9	2.6497	0.9885	0.0602–1.0329	58.39	2.5811
			2.4848	0.9113	0.0035–0.0602	41.61	

φ, porosity; K, permeability; D_i, fractal dimension corresponding to different scales of pore throats, $i = L$, macropore interval; $i = S$, micropore interval; F_i, different sizes of pore throats; T_r, ratio of pore throats at different sizes; D_C, comprehensive fractal dimension

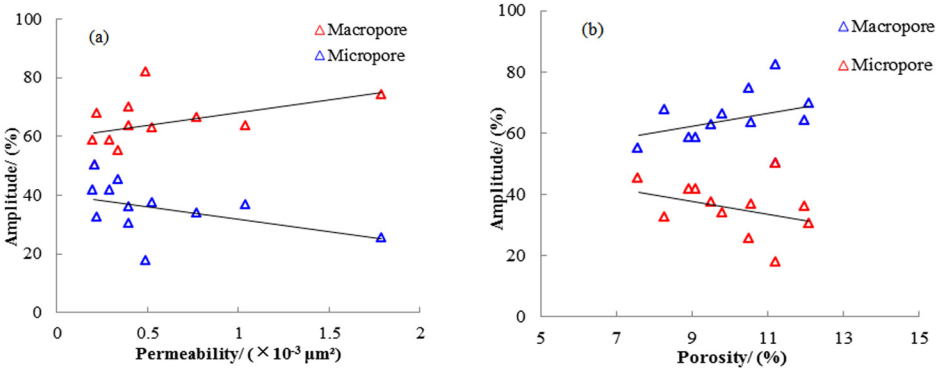

Figure 8: Relationship between permeability, porosity, and amplitude of pore distribution at different sizes. (a) the relationship curve between permeability and the amplitude of micropore and macropore; (b) the relationship curve between porosity and the amplitude of micropore and macropore.

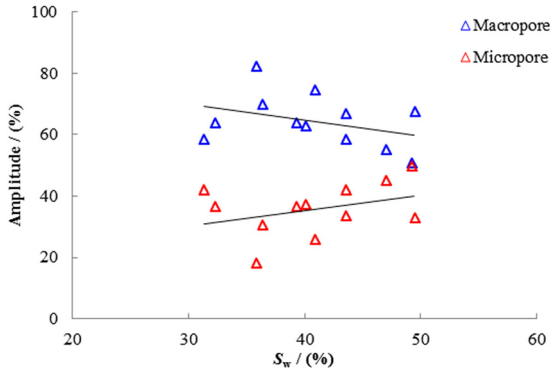

Figure 9: Relationship between S_w and distribution frequency of pore throats at different sizes.

of the tight sandstone in the target oilfield is between 2.5609 and 2.7364, with an average of 2.6696 (Table 3). However, the fractal dimension of the micropores (D_S) is between 2.0411 and 2.5526, with an average of 2.3256. Therefore, the fractal dimension of the large pore throat in the tight sandstone is larger than the fractal dimension of the micropore throat. This indicates that the structure of the micropore throat in the tight sandstone is relatively simple and the surface is relatively regular. The relative content of macropores and micropores in tight sandstone cores also can be derived. Among them, the proportion of macropores is 50.12 ~ 82.10%, with an average of 64.34%. The proportion of micropores is 17.90 ~ 49.88%, with an average of 35.66%. From Figure 8, as the permeability (Figure 8a) and porosity (Figure 8b) increase, the content of macropores in the core tends to increase. However, the proportion of micropores in the core shows a decreasing trend. In addition, the S_W obtained by HPMI test is a key parameter reflecting the ultimate oil recovery of oil and gas. S_W is mainly affected by the structure of the pore throat, so it can be used to characterize the pore throat structure of tight sandstone reservoirs. In tight sandstone reservoirs of E Basin, the S_W gradually decreases as the frequency of macropores increases and the S_W gradually increases as the frequency of small pores increases (Figure 9). This is related to the complexity of the pore structure of tight sandstone. The fractal dimension of large pores in tight sandstone is close to 3. According to fractal theory, the structure of macropores is more complicated than that of micropores in tight oil. Therefore, in the development of tight oil and gas, the impact of micropores on oil and gas seepage should be focused.

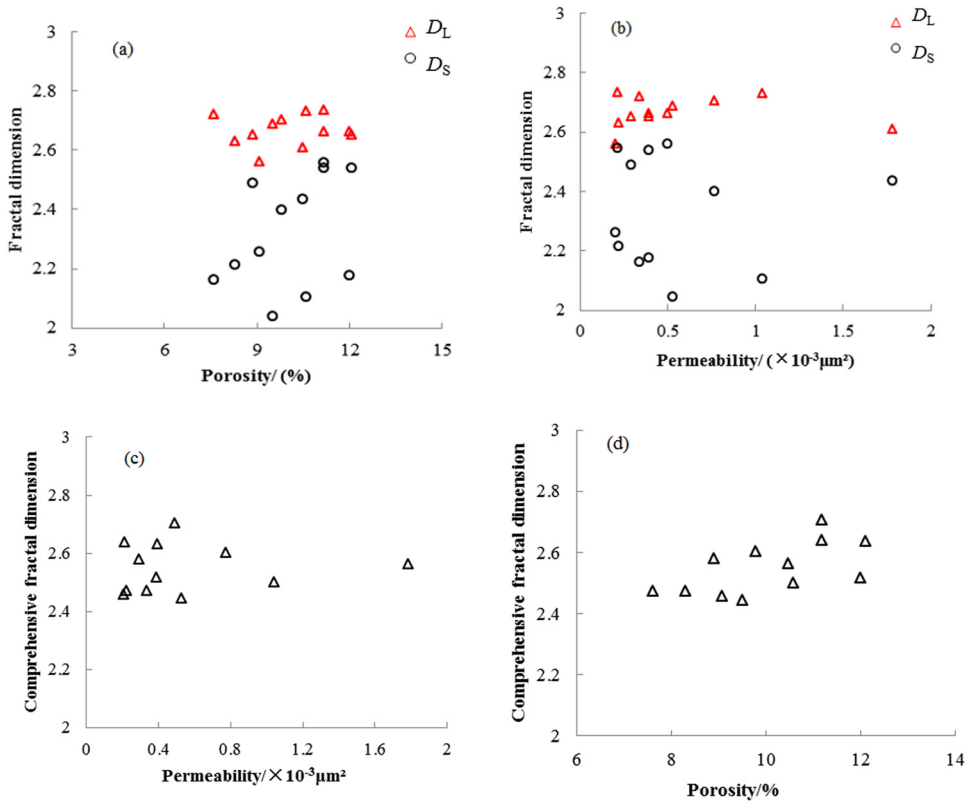

Figure 10: Relationship between fractal dimension (D_L, D_S, and D_c) and petrophysical properties of different sizes of pore throats.

5.2 Comprehensive fractal dimension and its application

Different sizes of pore throat have various fractal dimensions (D_S and D_L). Various fractal characteristics reflect the different properties of micropore throat structure, indicating the complexity of the pore throat structure of the tight sandstone in the E Basin. Zhao et al. proposed to characterize the fractal features of tight sandstones using comprehensive fractal dimensions. Its calculation formula is as follows [6]:

$$D_c = \sum D_i V_i \tag{11}$$

where D_c is the comprehensive fractal dimension, dimensionless number; D_i is the fractal dimension corresponding to the pore throat of different scales (macropores and micropores), namely D_L and D_S; V_i is the proportion of the pore throat corresponding to different fractal dimensions.

The D_c value calculated by equation (11) is between 2.4457 and 2.7034 with an average of 2.5483. Zhao et al. studied the comprehensive fractal dimension of tight sandstones in the Y Basin between 2.4294 and 2.6398, with an average of 2.5586 [6]. It can be found that the comprehensive fractal dimension of the tight sandstones in E Basin and Y Basin is basically same. And, the comprehensive fractal dimension values are close to the fractal dimension corresponding to the macropores (which fractal dimension is close to 3). Overall, the pore surface of the tight sandstone is rough, and the heterogeneity is serious. In addition, only the fractal dimension D_L corresponding to macropores throat has a positive correlation with permeability, which indicates that macropores' throat controls the permeability of tight sandstone (Figure 10b). There is no obvious correlation between D_S and D_c and permeability (Figures 10b and c). These suggest that the storage space of the different sizes of pore throat strongly controls the fractal characteristic. However, there is a positive correlation between porosity and fractal dimension. With the increase of porosity, the fractal dimension increases to a certain extent (Figure 10a and d). The analyses described previously reveal that D_L, D_S, and the total fractal dimension presented different correlations with corresponding porosity and permeability. This suggests that the pore throat structure of E Basin tight oil sandstone is complex and pore throat sizes strongly affect the fractal characteristics of the pore throat and its homogeneity and complexity.

6 Conclusion

In this work, we employed TS and HPMI technology to characterize the pore throat structure of tight sandstone in the E Basin. In addition, we fitted the fractal dimensions of different scales and calculated the comprehensive fractal dimension based on the HPMI. According to the accomplished results, the following conclusions can be drawn:

1. The tight sandstones of the E Basin have various types of cuttings, mainly metamorphic rocks and sedimentary rocks, including igneous rocks and mica, and soft cuttings are pseudo-matrices. In addition, the pore network of the tight oil sandstone mainly consists of primary pores, secondary pores, heterobasic pores, and microfractures.
2. The pore throat radius of the E Basin is between 0.0035 and 2.6158 μm, and its heterogeneity is strong. The tight sandstone pore throat radius distribution curve has two peaks, and as the permeability increases, the pore throat size distribution curve gradually shifts to the right.
3. The tight sandstones of the E Basin are characterized by segmentation fractals. According to the fractal features, the pores are divided into macropores (D_L) and micropores (D_S), and the values of the D_L and D_S are different. At the same time, the permeability and porosity are mainly contributed by the proportion of macropores, and the contribution of micropores to the permeability is relatively weak.
4. The comprehensive fractal dimension (D_c) is calculated and no correlation is found between permeability and porosity. In addition, the D_c of tight sandstones in E Basin and Y Basin is compared and found to be similar. And, the size of the integrated fractal dimension is close to the fractal dimension of the macropore interval.

Acknowledgments: The authors are grateful to Yapu Zhang, Zhongkun Niu, and Xinliang Chen, Exploration and Development Research Institute of SINOPEC North China Company, for their help during the TS analyses. This study was financially supported by the National Science and Technology Major Project (2017ZX05013-001) and the R&D of PetroChina Company Limited (2019B-1311).

Author contributions: Each author has made contributions to this paper. XLZ, ZMY, and XWL designed the experiments (HPMI and TS) and XLZ carried them out. XLZ, ZMY, XWL, and ZYW deduced the calculation formula of fractal dimension and fitted it with experimental data. XWL and YTL provide relevant insights into the part of the discussion. XLZ and XWL wrote and

edited the manuscript. All authors have read and approved the final manuscript.

References

[1] Liu H, Yang Y, Wang F, Deng X, Liu Y, Nan J, et al. Micro pore and throat characteristics and origin of tight sandstone reservoirs: a case study of the Triassic Chang 6 and Chang 8 members in Longdong area, Ordos Basin, NW China. Pet Explor Dev+. 2018;45(2):239–50.

[2] Zhao XL, Yang Z, Lin W, Xiong S, Luo Y, Wang Z, et al. Study on pore structures of tight sandstone reservoirs based on nitrogen adsorption, high-pressure mercury intrusion, and rate-controlled mercury intrusion. J Energ Resour-ASME. 2019;141(11):112903–11.

[3] Zou CN, Zhu R, Liu K, Su L, Bai B, Zhang X, et al. Tight gas sandstone reservoirs in China: characteristics and recognition criteria. J Pet Sci Eng. 2012;88:82–91.

[4] Zou CN, Zhang G, Yang Z, Tao S, Hou L, Zhu R, et al. Geological concepts, characteristics, resource potential and key techniques of unconventional hydrocarbon: on unconventional petroleum geology. Pet Explor Dev+. 2013;40(4):413–28.

[5] Wang Z, Yang Z, Ding Y, He Y, Lin W, Wang W, et al. A multi-linear fractal model for pressure transient analysis of multiple fractured horizontal wells in tight oil reservoirs including imbibition. Fractals. 2018;27(1):1940004.

[6] Zhao X, Yang Z, Lin W, Xiong S, Luo Y, Liu X, et al. Fractal study on pore structure of tight sandstone based on full-scale map. Int J Oil Gas Coal T. 2019;22(2):123–39.

[7] Song Z, Liu G, Yang W, Zou H, Sun M, Wang X. Multi-fractal distribution analysis for pore structure characterization of tight sandstone – a case study of the Upper Paleozoic tight formations in the Longdong District, Ordos Basin. Mar Pet Geol. 2018;92:842–54.

[8] Clarkson C, Freeman M, He L, Agamalian M, Melnichenko Y, Mastalerz M, et al. Characterization of tight gas reservoir pore structure using USANS/SANS and gas adsorption analysis. Fuel. 2012;95(1):371–85.

[9] Clarkson C, Solano N, Bustin R, Bustin A, Chalmers G, He L, et al. Pore structure characterization of North American shale gas reservoirs using USANS/SANS, gas adsorption, and mercury intrusion. Fuel. 2013;103:606–16.

[10] Zhao X, Yang Z, Lin W, Xiong S, Wei Y. Characteristics of microscopic pore-throat structure of tight oil reservoirs in Sichuan Basin measured by rate-controlled mercury injection. Open Phys. 2018;16:675–84.

[11] Li P, Zheng M, Bi H, Wu S, Wang X. Pore throat structure and fractal characteristics of tight oil sandstone: a case study in the Ordos basin, China. J Pet Sci Eng. 2017;149:665–74.

[12] Toledo P, Scriven L, Davis H. Pore-space statistics and capillary pressure curves from volume-controlled porosimetry. SPE Form Eval. 1994;9:46.

[13] Cao Z, Liu G, Zhan H, Li C, You Y, Yang C, et al. Pore structure characterization of Chang-7 tight sandstone using MICP combined with N2GA techniques and its geological control factors. Sci Rep. 2016;6:36919.

[14] Labani M, Rezaee R, Saeedi A, Hinai A. Evaluation of pore size spectrum of gas shale reservoirs using low pressure nitrogen adsorption, gas expansion and mercury porosimetry: a case study from the Perth and Canning basins, western Australia. J Pet Sci Eng. 2013;112(3):7–16.

[15] Lai J, Wang G, Chai Y, Xin Y, Wu Q, Zhang X, et al. Deep burial diagenesis and reservoir quality evolution of high-temperature, high-pressure sandstones: examples from Lower Cretaceous Bashijiqike Formation in Keshen area, Kuqa depression, Tarim basin of China. AAPG Bull. 2017;101(6):829–62.

[16] Xiao D, Lu Z, Jiang S, Lu S. Comparison and integration of experimental methods to characterize the full-range pore features of tight gas sandstone – a case study in Songliao basin of China. J Nat Gas Sci Eng. 2016;34:1412–21.

[17] Nabawy B, David C. X-ray CT scanning imaging for the Nubia sandstone as a tool for characterizing its capillary properties. Geosci J. 2016;20(5):1–14.

[18] Zhao P, Wang Z, Sun Z, Cai J, Wang L. Investigation on the pore structure and multifractal characteristics of tight oil reservoirs using NMR measurements: Permian Lucaogou formation in Jimusaer sag, Junggar Basin. Mar Pet Geol. 2017;86:1067–81.

[19] Xiao D, Jiang S, Thul D, Lu S, Zhang L, Li B. Impacts of clay on pore structure, storage and percolation of tight sandstones from the Songliao Basin, China: implications for genetic classification of tight sandstone reservoirs. Fuel. 2018;211:390–404.

[20] Shao X, Pang X, Li H, Zhang X. Fractal analysis of pore network in tight gas sandstones using NMR method: a case study from the Ordos Basin, China. Energy Fuel. 2017;31:10358–68.

[21] Lai J, Wang G, Wang Z, Chen J, Pang X, Wang S, et al. A review on pore structure characterization in tight sandstones. Earth-Sci Rev. 2018;177:436–57.

[22] Gao H, Jing X, Zhang L. Difference of micro-pore throat characteristics in extra-low permeability sandstone of different pore throat matching relationship. Pet Geol Exp. 2013;35:401–6.

[23] Yang R. Adsorbents: fundamentals and applications. Hoboken, NJ: John Wiley &Sons; 2003.

[24] Shen W, Li X, Lu X, Guo W, Zhou S, Wan Y. Experimental study and isotherm models of water vapor adsorption in shale rocks. J Nat Gas Sci Eng. 2018;52:484–91.

[25] Tokunaga T, Shen W, Wan J, Kim Y, Cihan A, Zhang Y, et al. Water saturation relations and their diffusion-limited equilibration in gas shale: implications for gas flow in unconventional reservoirs. Water Resour Res. 2017;53:9757–70.

[26] Wu H, Zhang C, Ji Y, Liu R, Wu H, Zhang Y, et al. An improved method of characterizing the pore structure in tight oil reservoirs: integrated NMR and constant-rate-controlled porosimetry data. J Pet Sci Eng. 2018;166:778–96.

[27] Wilkinson M, Haszeldine R, Morton A, Fallick A. Deep burial dissolution of k-feldspars in a fluvial sandstone, Pentland formation, UK central North Sea. J Geol Soc. 2014;171(5):635–47.

[28] Hakimi M, Shalaby M, Abdullah W. Diagenetic characteristics and reservoir quality of the Lower Cretaceous Biyadh sandstones at Kharir oilfield in the western central Masila Basin, Yemen. J Asian Earth Sci. 2012;51:109–20.

[29] Mayo S, Josh M, Nesterets Y, Esteban L, Pervukhina M, Clennell M, et al. Quantitative micro-porosity characterization

using synchrotron micro-CT and xenon K-edge subtraction in sandstones, carbonates, shales and coal. Fuel. 2015;154:167–73.
[30] Zhang F, Jiang Z, Sun W, Li Y, Zhang X, Zhu L, et al. A multiscale comprehensive study on pore structure of tight sandstone reservoir realized by nuclear magnetic resonance, high pressure mercury injection and constant-rate mercury injection penetration test. Mar Pet Geol. 2019;109:208–22.
[31] Yu Y, Luo X, Wang Z, Cheng M, Lei Y, Zhang L, et al. A new correction method for mercury injection capillary pressure (MICP) to characterize the pore structure of shale. J Nat Gas Sci Eng. 2019;68:102896.
[32] Celeste D, Paul C. Using mercury injection pressure analyses to estimate sealing capacity of the Tuscaloosa marine shale in Mississippi, USA: implications for carbon dioxide sequestration. Int J Greenh Gas Con. 2018;78:375–87.
[33] Schlueter E, Zimmerman R, Witherspoon P, Cook N. The fractal dimension of pores in sedimentary rocks and its influence on permeability. Eng Geol. 1997;48(3):199–215.
[34] Mandelbrot B, Passoja D, Paullay A. Fractal character of fracture surfaces of metals. Nature. 1984;308:721–2.
[35] Wang H, Liu Y, Song Y, Zhao Y, Zhao J, Wang D. Fractal analysis and its impact factors on pore structure of artificial cores based on the images obtained using magnetic resonance imaging. J Appl Geophys. 2012;86:70–81.
[36] Zhang L, Lu S, Xiao D, Li B. Pore structure characteristics of tight sandstones in the northern Songliao Basin, China. Mar Pet Geol. 2017;88:170–80.
[37] Lin W, Li X, Yang Z, Lin L, Xiong S, Wang Z, et al. A new improved threshold segmentation method for scanning images of reservoir rocks considering pore fractal characteristics. Fractals. 2018;26(2):1840003.
[38] Lin W, Yang Z, Li X, Wang J, He Y, Wu G, et al. A method to select representative rock samples for digital core modeling. Fractals. 2017;25(4):1740013.
[39] Wang F, Cheng Y, Lu S, Jin K, Zhao W. Influence of coalification on the pore characteristics of middle-high rank coal. Energy Fuels. 2014;28(9):5729–36.
[40] Xie S, Cheng Q, Ling Q, Li B, Bao Z, Fan P. Fractal and multifractal analysis of carbonate pore-scale digital images of petroleum reservoirs. Mar Pet Geol. 2010;27:476–85.
[41] Brunauer S, Deming L, Deming W, Teller E. On a theory of the van der Waals adsorption of gases. Am Chem Soc. 1940;62(7):1723–32.
[42] Zhao H, Ning Z, Wang Q, Zhang R, Zhao T, Niu T, et al. Petrophysical characterization of tight oil reservoirs using pressure-controlled porosimetry combined with rate-controlled porosimetry. Fuel. 2015;154:233–42.
[43] Pittman ED. Relationship of porosity and permeability to various parameters derived from mercury injection capillary pressure curves for sandstones. AAPG Bull. 1992;76(2):191–8.
[44] Loucks R, Reed R, Ruppel S, Hammes U. Spectrum of pore types and networks in mudrocks and a descriptive classification for matrix-related mudrock pores. AAPG Bull. 2012;96:1071–98.
[45] Washburn W. The dynamics of capillary flow. Phys Rev. 1921;17:273–83.
[46] Li K. Analytical derivation of Brooks–Corey type capillary pressure models using fractal geometry and evaluation of rock heterogeneity. J Pet Sci Eng. 2010;73(1–2):20–6.
[47] Wang F, Yang K, You J, Lei X. Analysis of pore size distribution and fractal dimension in tight sandstone with mercury intrusion porosimetry. Res Phys. 2019;13:102283.
[48] Panahi H, Kobchenko M, Meakin P, Dysthe D, Renard F. Fluid expulsion and microfracturing during the pyrolysis of an organic rich shale. Fuel. 2019;235:1–16.
[49] Song Z, Hou J, Zhang L, Chen Z, Li M. Experimental study on disproportionate permeability reduction caused by non-recovered fracturing fluids in tight oil reservoirs. Fuel. 2018;226:627–34.
[50] Xi K, Cao Y, Haile B, Zhu R, Jahren J, Bjørlykke K, et al. How does the pore-throat size control the reservoir quality and oiliness of tight sandstones? The case of the Lower Cretaceous Quantou Formation in the southern Songliao Basin, China. Mar Pet Geol. 2016;76:1–15.